Nanoparticles: Scaffolds and Building Blocks

ROY SHENHAR AND VINCENT M. ROTELLO*
Department of Chemistry, University of Massachusetts, Amherst, Massachusetts 01003

Received October 23, 2002

ABSTRACT
Nanoparticles provide key tools for bridging the gap between "bottom-up" synthetic methods and "top-down" fabrication. In this Account we describe some of the unique structural aspects of nanoparticles and the use of these attributes to the creation of devices with tunable specificity and environmental response. We also explore the use of nanoparticles as "building blocks" for the creation of nanocomposite materials that feature structural control from the molecular to the micron scale.

I. Introduction

Multiscale fabrication is a crucial goal in nanotechnology. Top-down fabrication methods such as photo- and electron-beam lithography provide a tool for etching surfaces to provide structures on the nanometer scale.[1] Two- and three-dimensional structures can be formed using lithography, but these structures, however, are limited by the inherent two-dimensionality of each lithographic step. Bottom-up methods using the techniques of organic and inorganic synthesis furnish a means of fabricating molecular systems such as devices and sensors that are on the 0.5−2.5 nm scale with complete control of three-dimensional structure.[2] Synthesis and lithography provide complementary tools for nanotechnology, but the integration of these techniques remains a significant challenge.

Nanoparticle systems, including monolayer-protected clusters (MPCs) and mixed monolayer-protected clusters (MMPCs),[3] bridge the gap between lithographic and synthetic methods (Figure 1). MPCs are core−shell type systems that feature a self-assembled monolayer (SAM)-functionalized metallic or semiconductor core. The monolayer coverage provides two key functions: shielding the particles from agglomeration and furnishing a scaffold for the attachment of functional molecular entities. MMPCs greatly extend the versatility of core−shell systems, providing multiple functionalities on the monolayer shell.

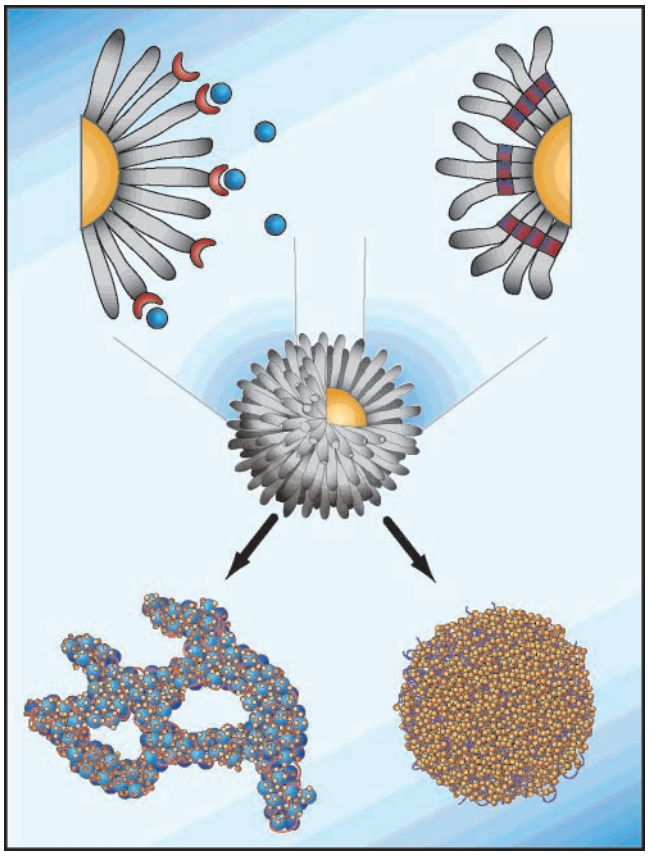

FIGURE 1. Nanoparticles as scaffolds for molecular-level control of properties and as building blocks in macroscopic assemblies.

The fabrication of MPC and MMPC systems has been greatly facilitated by the methods developed by Brust et al.[4] In their approach chemical reduction of metal salts (Pd, Au, Ag, Pt) is performed in the presence of capping ligands (Figure 2). The mild conditions and moderate reducing agents used in this process are compatible with a wide range of ligand functionality. The size of nanoparticles can be controlled through the stoichiometry of the metal salt to capping ligand, providing MPCs and MMPCs ranging in size from 1.5 to 8 nm and overall diameters of 2.5−11 nm.[5] These nanoparticles can be further elaborated through ligand displacement (Figure 2). Repeating this step with different ligands leads to multifunctional MMPCs. This is a potent technique for obtaining structural diversity, providing rapid generation of a wide variety of MMPC systems.[6]

Nanoparticles themselves also provide a pragmatic approach to the challenge of multiscale engineering, functioning as "building blocks" of regular shape and size for the fabrication of larger structures. Combination of synthetic design with directed assembly of nanoparticles into ensembles provides direct control of structure from the molecular to the macroscopic level.

Roy Shenhar was born in 1971 in Rehovot, Israel. After receiving his B.Sc. in Chemistry and Computer Science from the Hebrew University of Jerusalem in 1995, he continued onto a Ph.D. in Chemistry, which he obtained with Mordecai Rabinovitz and Itamar Willner in 2002. Currently a Fulbright Postdoctoral Research Associate in Prof. Rotello's Group at the University of Massachusetts, his interests span the areas of self-assembly, nanoparticle, and polymer chemistry. His current research is focused on the combination of molecular recognition with nanoparticles and block copolymers.

Vincent Rotello received his B.S. from Illinois Institute of Technology in 1985. He obtained his Ph.D. in 1990 from Yale University with Harry Wasserman. From 1990 to 93, he was an NSF postdoctoral fellow with Julius Rebek Jr. at M.I.T. Since 1993, Professor Rotello has been at the University of Massachusetts at Amherst as an Assistant (1993−1998), Associate (1998−2001), and Professor (2001−) of Chemistry, with appointments in Polymer Science and Engineering and in the Program in Molecular and Cellular Biology. He has been the recipient of the NSF CAREER and the Cottrell Scholar Award, as well as the Camille Dreyfus Teacher−Scholar and the Sloan Fellowship. His research focuses on the application of molecular recognition to devices, polymers, nanotechnology, and biological systems.

10.1021/ar020083j CCC: $25.00
Published on Web 05/23/2003

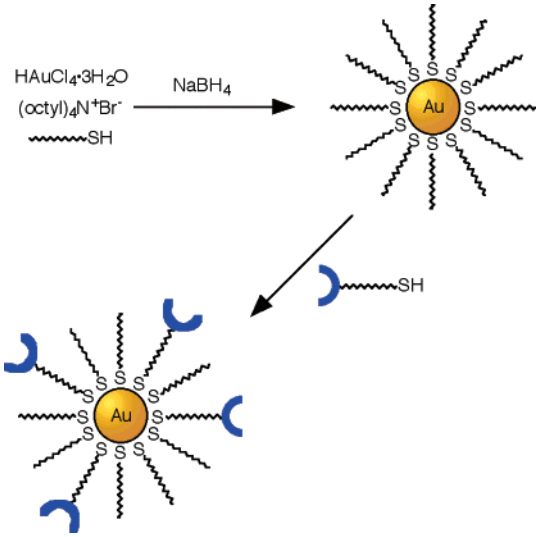

FIGURE 2. Synthetic route to Au MPCs and MMPCs. Nanoparticles featuring other cores (Pd, Pt) can be formed in analogous fashion.

II. Structural Attributes of Monolayer Protected Clusters

The ease of fabrication of MPCs and MMPCs, combined with the ability to characterize these systems using standard solution-phase techniques such as nuclear magnetic resonance (NMR), infrared (IR), and UV−vis spectroscopies, makes nanoparticles obvious starting points for device fabrication. First, however, we must become familiar with the unique characteristics provided by the MPC scaffold.

One unique structural characteristic that is inherent in nanoparticle cores is faceted surfaces, which generate a radial structure for the covering SAM.[3,5] To explore the consequences of this radial structure, we have fabricated MPCs **1**−**5** featuring amide side chains at varying positions along the chains.[7] Hydrogen-bonding efficiency was monitored through the N−H stretching frequency (Figure 3). In MPC **1**, where the amide functionalities are close to the gold surface, inefficient hydrogen bonding is observed (a relatively high N−H stretching frequency) due to the high conformational demand imposed on the side chains, which does not exist in the analogous amide **6** (Figure 4). The hydrogen-bonding interaction is most enhanced in MPC **2** and gradually decreases as the gold surface-amide distance increases (MPC **3**−**5**). This radial dependence arises from the increased entropy as the side chains diverge (Figure 4).

The radial dependence shown above provides a means of controlling the assembly of the protecting monolayer. The varying chain density also dictates the appearance of the nanoparticle outer surface; end-group structure can be used to control monolayer assembly by projecting the surface-packing mode into the monolayer arrangement. We have synthesized amide-functionalized MPCs **7a**−**d** (Figure 5) bearing end-groups of varying steric bulk (**7b**−**d**) and π-stacking ability (**7a**).[8] We then used the amide function to probe the influence of the nature of the end-group on the hydrogen-bonding efficiency and independently tested the protection provided by the monolayer-

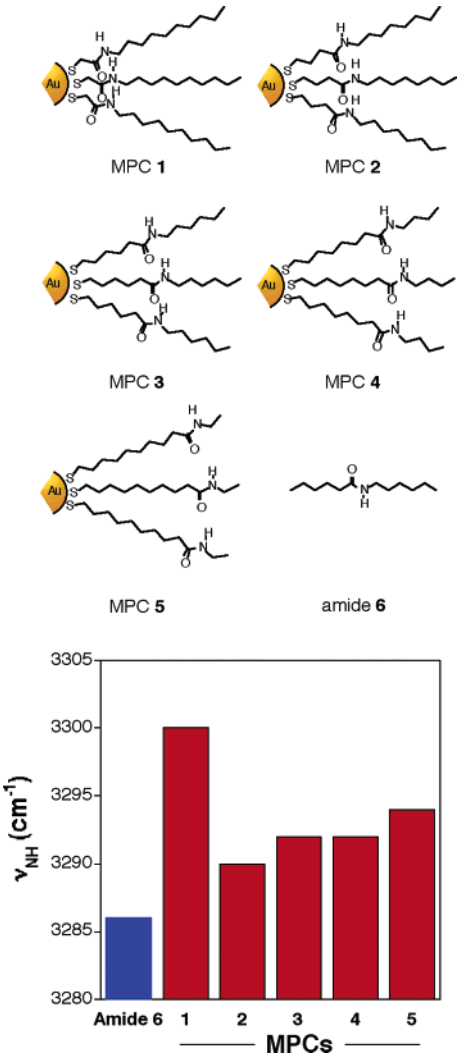

FIGURE 3. N−H stretching frequencies of MPCs **1**−**5** and amide **6**.

packing mode against cyanide-induced decomposition.[9] Both hydrogen-bonding efficiency and resistance toward NaCN degradation decrease in the order diphenylmethyl > isobutyl > propyl > *tert*-butyl (Figure 5). This behavior is attributed to the packing quality at the periphery, which has similar influence both on chain pre-alignment and on nanoparticle shielding. Enhanced packing is demonstrated with favorably interacting end-groups (diphenylmethyl), while isopropyl end-groups provide better steric packing than propyl end groups, and *tert*-butyl groups, on the other hand, cause surface overcrowding that distorts the chains.

NaCN decomposition studies of corresponding ester analogues **8a**, **8c**, and **8d** show markedly slower decomposition rates compared to the amide derivatives. Additionally, the end-group effect, although following the same trend as with the amides, is much weaker (Figure 5). This ostensible contradiction to the enhanced stability observed in amide-functionalized flat SAMs[10] reveals the crucial role of uniform chain-density gradient in nanoparticle stabilization and suggests a "vertex effect" arising from the faceted nature of the gold cluster surface. The vertexes are the most reactive sites on the core surface.[5,11]

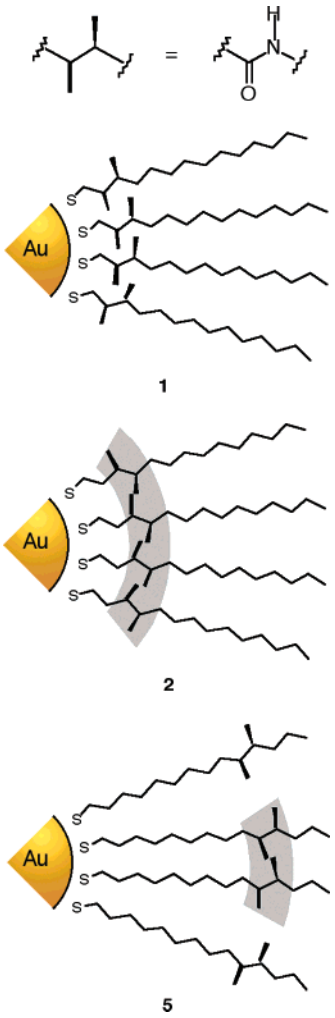

FIGURE 4. Monolayer packing and hydrogen bonding in MPCs **1**, **2**, and **5**. Gray stripes represent hydrogen-bonding regions.

Hydrogen bonding in the amide-nanoparticles form facet-segregated bundles, exposing the vertexes to CN^- penetration (Figure 6a). Adequate peripheral end-groups allow extension of the hydrogen-bonding network over some of the vertexes (Figure 6b); nevertheless, it is the uniform chain-density gradient exhibited by the ester MPCs that ultimately provides the best protection (Figure 6c).

III. Device Fabrication using Nanoparticle Scaffolds

The ability to control the behavior of the nanoparticle monolayer raises the possibility of using MPCs as scaffolds for a variety of systems. For example, the fine-tuning of the hydrogen-bonding interaction may be used to control the dynamic features of proton-transfer reactions and their catalysis. To test this hypothesis, we analyzed colloids **2**−**5** and amide **6** for hydrogen/deuterium (H/D) exchange with CD_3OD, with and without the presence of catalytic amounts of acid.[12] Significantly slower exchange rates are observed for the MPCs featuring more deeply buried and hydrogen-bonded amide functionalities, whereas the exposed amide **6** shows the fastest H/D exchange when no

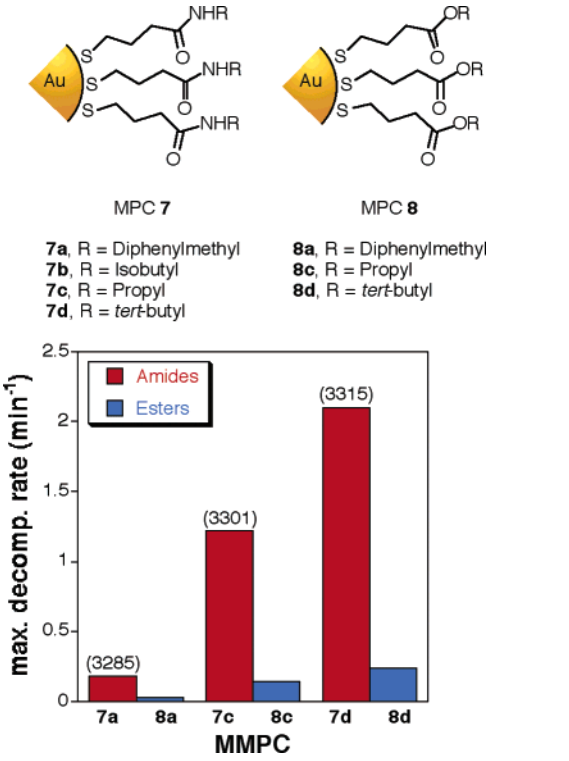

FIGURE 5. Maximal NaCN decomposition rates of amide- and corresponding ester-functionalized MPCs. For comparison, N−H stretching frequencies (cm^{-1}) of the corresponding amide-functionalized MPCs are given in parentheses.

acid is added (Figure 7). This trend arises from a combination of the hydrogen-bonding strength and the solvent inaccessibility due to steric hindrance of the shielding alkyl chains. Addition of catalytic amounts of *p*-toluenesulfonic acid dramatically accelerates the H/D exchange in MPCs **2**−**5**, while practically no effect due to added acid is observed for **6** (Figure 7). In fact, the maximum rate increase for colloids **4** and **5** actually exceeds the exchange rate for the "naked" control **6** under identical conditions. This is a result of catalysis provided by the hydrogen-bonding environment of the monolayer,[13] as evident by the clear correlation between the maximum relative rates achieved and the hydrogen-bonding strength. These results point the way for these systems to be used as biomimetic catalysts through proper engineering.

The ability to specifically interact with other molecules would further demonstrate the function of MPCs as molecular devices. We began the exploration of this aspect by the creation of MMPC **9**,[14] a monotopic receptor for flavin utilizing the diamidopyridine (DAP)-flavin three-point hydrogen bonding (Figure 8a). The choice of redox-active flavin (Figure 8b) as the guest provided the potential for electroactive device fabrication.[15]

Recognition between flavin (Fl_{ox}) and MMPC **9** was quantified in chloroform by following the ^1H NMR shifts of Fl_{ox}. The resulting shifts cleanly fit a 1:1 binding isotherm, from which an association constant (K_a) of 196 ± 8 M^{-1} was calculated, well within the range 150−500 M^{-1} observed in previous studies of free diamidopyridines.[15]

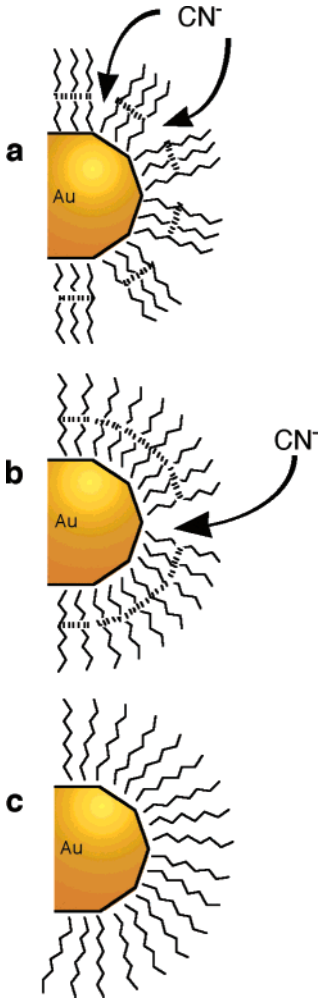

FIGURE 6. Vertex effect on decomposition rates of amide- and ester-functionalized MPCs: (a) weakly hydrogen-bonded systems; (b) strongly hydrogen-bonded systems; (c) ester colloids.

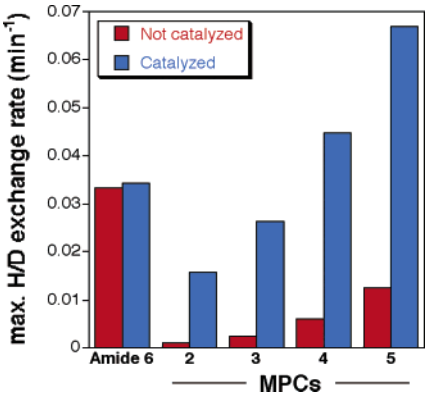

FIGURE 7. Maximum H/D noncatalyzed and catalyzed (*p*-toluenesulfonic acid) exchange rates for colloids **2**−**5** and amide **6**.

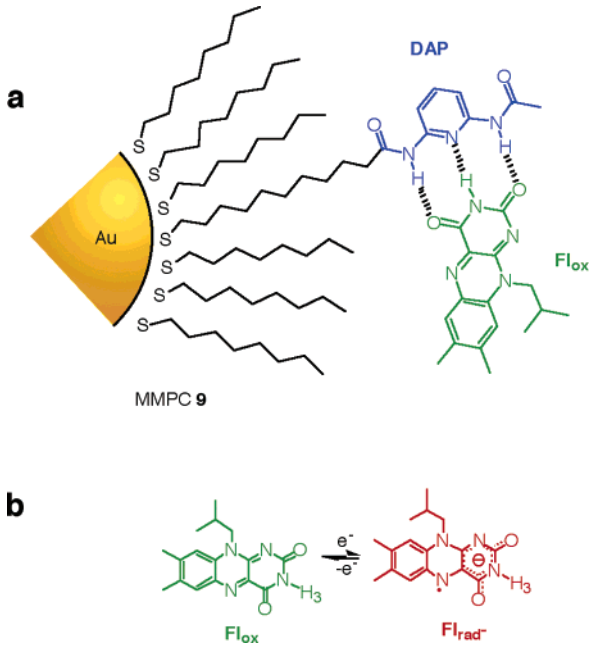

FIGURE 8. (a) Three-point hydrogen bonding between flavin and diamidopyridine-functionalized MMPC **9**. (b) Reduction of Fl_{ox} to Fl_{rad-}.

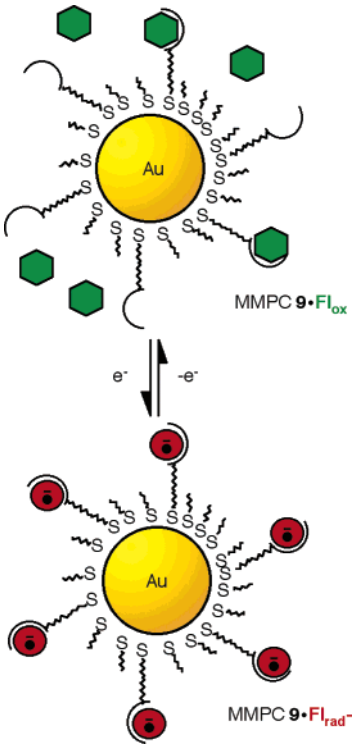

FIGURE 9. Schematic representation of the electrochemically controlled recognition of flavin by MMPC **9**.

The response of MMPC **9** toward reduction of Fl_{ox} to Fl_{rad-} was quantified using voltammetric methods.[15] The reduction potential of flavin was positively shifted by 81 mV upon addition of MMPC **9**, corresponding to a 20-fold stronger binding of Fl_{rad-} compared to Fl_{ox}, from 196 to 4500 M^{-1}.[16] This redox control of recognition represents a direct electrochemical switch for the manipulation of nanoparticle surface (Figure 9). Significantly, these experiments demonstrate that MMPCs provide a versatile and characterizable intermediate between solution devices and surface-based assemblies.

We next turned to the investigation of MMPCs featuring multivalent recognition sites designed to enhance the specificity of MPCs toward guest molecules through multitopic recognition. To explore this possibility, we created MMPC **10** that features both DAP hydrogen-

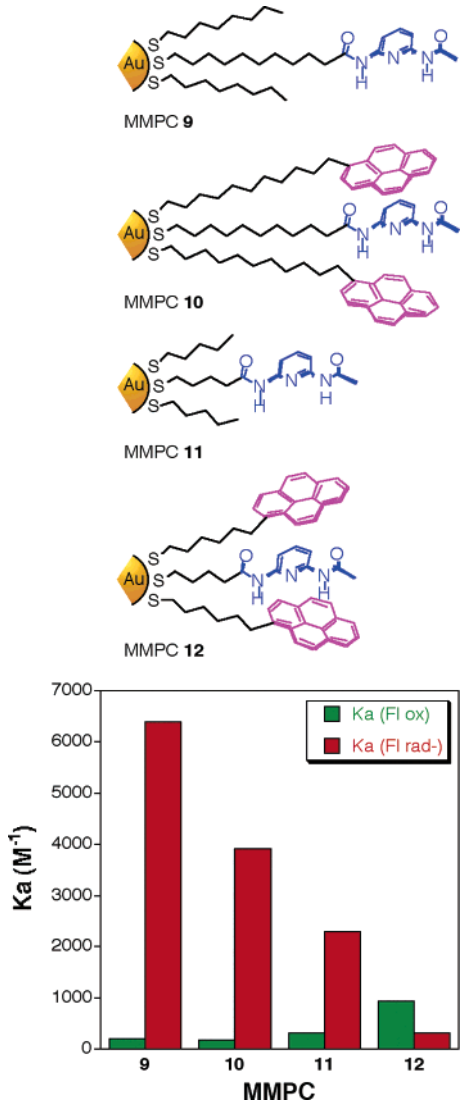

FIGURE 10. Association constants (K_a) of Fl_{ox} and Fl_{rad-} with MMPCs **9**−**12** in CH_2Cl_2.

bonding moieties and pyrene (Pyr) aromatic stacking elements.[17] In this MMPC, recognition of the electron deficient Fl_{ox} is obtained both through hydrogen bonding to the DAP units (as in MMPC **9**), and additionally through favorable π-stacking with the electron-rich pyrene units. As a result of this multitopic interaction, the binding constant of flavin with MMPC **10** is 323 ± 20 M^{-1}, nearly 2-fold greater than that when MMPC **9** is used.

The ability to radially govern functional group disposition provides further control of multivalent interactions at the particle surface. To demonstrate this capability, we synthesized MMPCs **11** and **12**,[18] which are analogous to MMPCs **9** and **10** but have shorter chains, thus providing a much denser environment for the functionalities embedded in the monolayers. MMPCs **9** and **11** bind flavin through hydrogen bonding alone, and bifunctional MMPCs **10** and **12** feature multivalent hydrogen bonding and aromatic stacking. Figure 10 shows the binding constants observed for MMPCs **9**−**12** with Fl_{ox} and Fl_{rad-}. As expected, there is essentially no radial dependence for the monovalent recognition of Fl_{ox} by monotopic MMPCs **9** and **11**. In contrast, multivalent recognition with MMPCs **10** and **12** exhibits a strong radial effect, with the shorter and more pre-organized host **12** binding Fl_{ox} 3-fold more efficiently than MMPC **10**.

To make matters more interesting (albeit more complicated), we explored the redox chemistry of our mono- and multitopic MMPCs. Reduction of Fl_{ox} to Fl_{rad-} inverts the trend observed with Fl_{ox}. On one hand, Fl_{rad-} hydrogen-binds more efficiently to DAP due to enhanced hydrogen acceptor abilities of the two carbonyl groups,[15] resulting in higher binding constants of MMPCs **9**−**11** with Fl_{rad-} compared to that with Fl_{ox}. In contrast, the reduction transforms the flavin moiety into an electron rich system, rendering the interaction with pyrene unfavorable. This effect is evident from the marked decrease in the binding constants of Fl_{rad-} with ditopic MMPCs **10** and **12** compared to with monotopic MMPCs **9** and **11**. The radial dependence plays a more crucial role in the ditopic systems: With MMPCs **9** and **11**, there is only a moderate (<3-fold) preference for the binding with the longer chain systems (mainly due to steric effects), whereas the repulsive aromatic interactions cause a 12-fold decrease in the binding constant with MMPC **12** compared to with MMPC **10**. In fact, the unfavorable aromatic interaction in MMPC **12** overrides the reduction-enhanced hydrogen-bonding affinity and becomes the major effect, as this system prefers the binding to Fl_{ox} rather than to Fl_{rad-}. This is a direct consequence of the chain density gradient, which is a function of the alkane chain lengths used. The 11-carbon chains in MMPC **10** have enough conformational freedom to enable them to accommodate and minimize repulsive interactions occurring between end-groups by moving the pyrene units away from the hydrogen-bound Fl_{rad-} (Figure 11a). This is, however, not possible for MMPC **12**, where the 6-carbon chains form a much tighter environment, providing a system incapable of relieving the repulsive interactions (Figure 11b).

One important feature of MPC systems that can be harnessed for the creation of even more sophisticated and selective molecular receptors is the mobility of thiols on the SAM surface.[11,19] This feature raises the possibility of creating environmentally responsive systems, in which maximization of interaction enthalpy would serve as the driving force for dynamic optimization of host−guest interactions. To explore the possibility of creating templatable hosts, we incorporated DAP moieties in a colloid protected by a mixed monolayer of both pyrene−alkanethiols and octanethiols, forming MMPC **13**.[17] The binding between flavin and MMPC **13** (and MMPC **9**, used as a control) in chloroform was monitored through shifts in the magnetic resonances of flavin over a 73 h period at constant concentrations. Essentially no change is observed when flavin is bound to MMPC **9**. However, upon binding to MMPC **13**, the chemical shift of the flavin N(3)H moves smoothly downfield by ~200 ppb, corresponding to an increase in the colloid−flavin recognition. Concomitantly, the C(6)H resonance is gradually shifted upfield, indicative of the enhanced aromatic stacking provided by binding site optimization. The evolving picture is the following

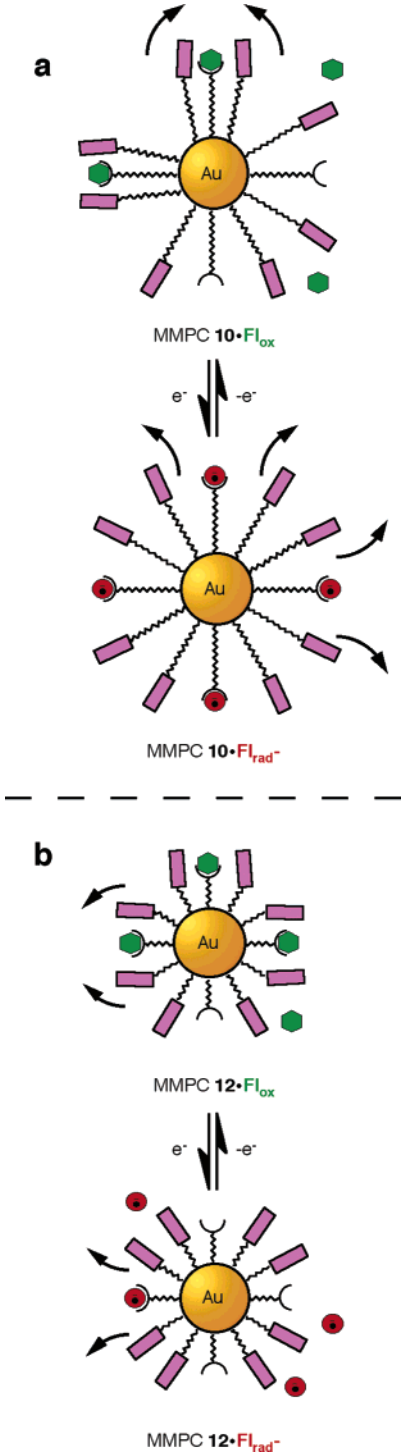

FIGURE 11. Schematic illustration of the chain length effect on the redox modulated binding of Fl_{ox}/Fl_{rad-} to multivalent MMPCs with (a) long chain spacers, (b) short chain spacers.

(Figure 12): Initially, the DAP and pyrene units are randomly distributed within the octanethiol monolayer, giving rise to an initial binding constant with flavin of 168 M^{-1}. Once the flavin is bound to a DAP moiety on the monolayer, the pyrene−thiols self-organize to maximize binding enthalpy, giving rise to the changes in the NMR spectra, from which an increase in K_a to 235 M^{-1} (a 71% enhancement) is calculated.

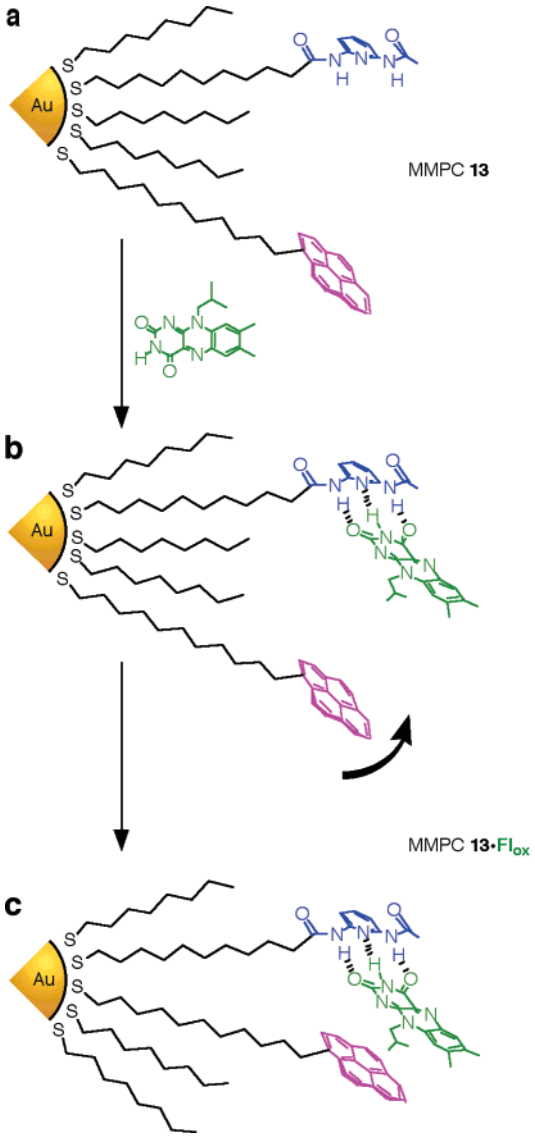

FIGURE 12. Flavin-mediated templation of MMPC **13**. (a) Initially, recognition elements are randomly distributed on the MMPC's surface. (b) Immedately after addition of flavin. (c) After incubation, recognition elements assemble into multi-topic binding pockets.

This guest-mediated templation provides a unique tool for the creation of surfaces tailored to bind specific biomacromolecules, making MMPCs potential leads for the creation of biosensors and for chemotherapeutics. We are currently working on creating sensors and therapeutics based on double stranded DNA[20] and protein recognition.[21] Concurrently, we are working to develop tools for regulating monolayer structure to further enhance the imprinting process.

IV. Nanoparticles as Building Blocks for Materials Fabrication

Nanoparticles can simultaneously provide scaffolds for devices and serve as building blocks for the creation of extended two- and three-dimensional systems.[22] The existing tools for the fabrication of nanoparticle assemblies are far less established than what conventional molecular synthesis provides for the creation of molecular systems.

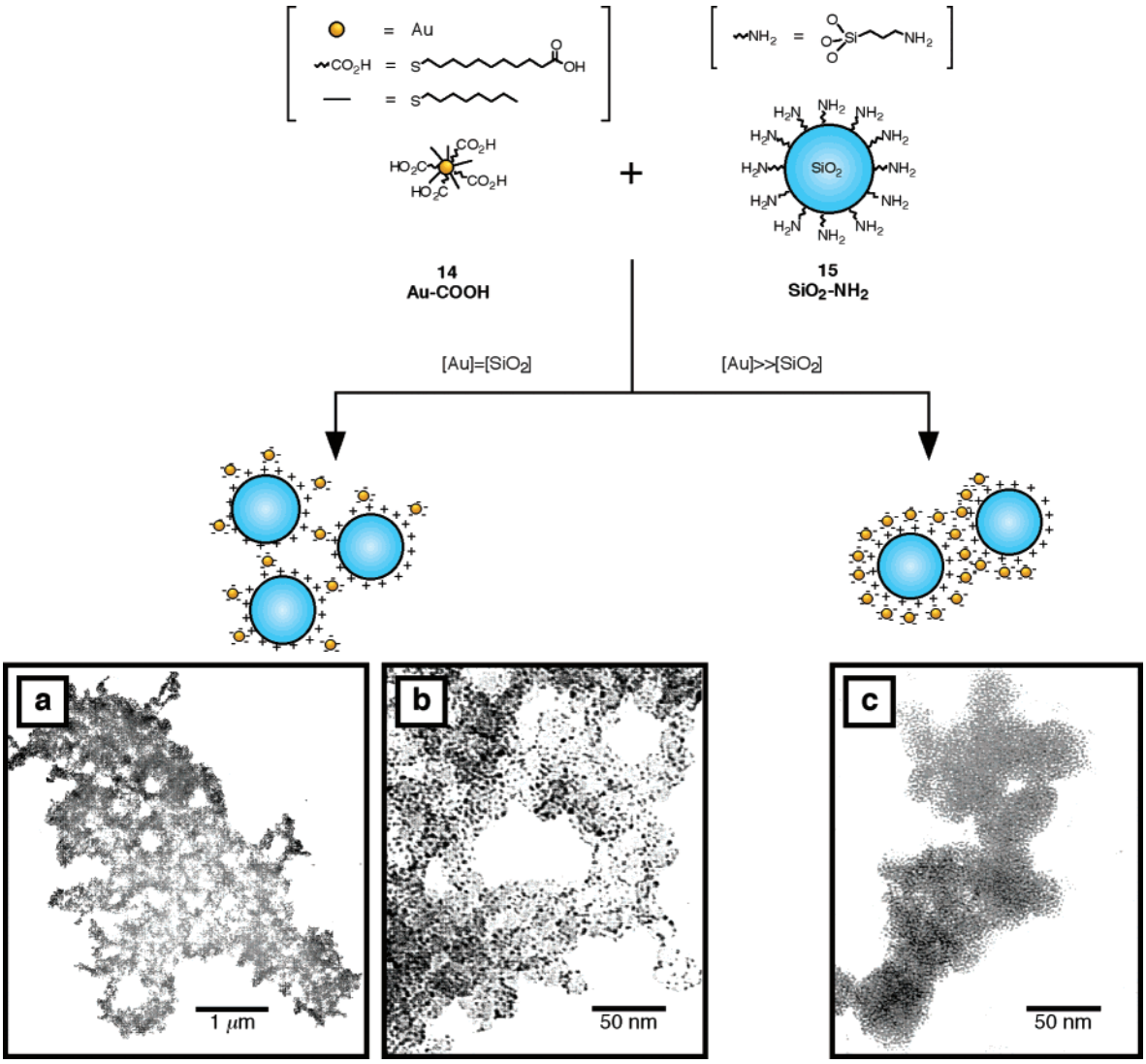

FIGURE 13. Nanocomposites assembled by the building block approach. (a and b) Large nanoparticle assembly formed by 1:1 (w/w) Au-COOH/SiO_2-NH_2 mixture. (c) Smaller-scale aggregate formed from 100:1 (w/w) Au-COOH/SiO_2-NH_2.

Our research is focused on addressing this imbalance and has centered on the creation of two distinct assembly morphologies: open-framework structures for catalytic applications and highly organized structures for use in multiscale engineering.

A. Nanoparticle Assemblies for Catalytic Applications. Noble metals catalyze numerous important reactions, including hydrogenation, oxidation, and Heck coupling.[23] The cost of these metals is high, making a high surface area-to-volume ratio a prerequisite for the creation of effective heterogeneous catalysts. A general method for achieving such high ratios is to precipitate the metal as colloidal particles onto preformed solid supports. Using this method, however, it is difficult to control particle size and disposition. Using our ability to modify and manipulate the surface of nanoparticles we sought an alternative method, based on "bottom-up" assembly of the colloidal particles.

In our first demonstration of the feasibility of a building block approach, we investigated the self-assembly of 2 nm carboxylic acid-functionalized gold colloids Au-COOH **14** and 15 nm amine-functionalized silica colloids SiO_2-NH_2 **15** (Figure 13).[24] Combining solutions of Au-COOH and SiO_2-NH_2 results in rapid formation of extended binary aggregates, in which larger SiO_2 particles are surrounded by smaller gold nanoparticles that appear regularly spaced (Figure 13b), presumably due to repulsive Coulombic interactions between charge-paired units. Increasing the Au-COOH fraction results in smaller aggregates with much denser surface coverage of the silica particles by gold nanoparticles (Figure 13c) resulting from the stoichiometry and the limited ionization of the carboxylic groups.

The two-component controlled assembly method uses the large SiO_2 particles as a scaffold for the Au colloids, providing highly open structures that exhibit both porosity and high exposure of the metal surface, making them reasonable starting points for catalyst design. Nevertheless, when the metal particle itself serves as glue, much of this expensive component remains inaccessible and becomes wasted. To both liberate the catalytic material and further enhance the control over aggregate morphology, we added a flexible polymeric mediator.[25] This

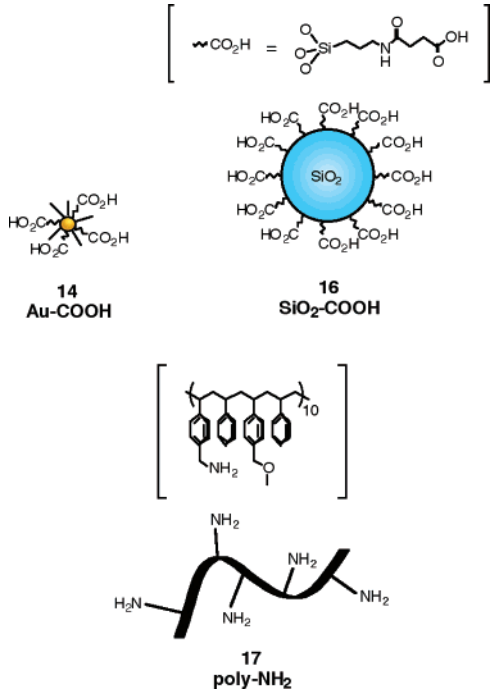

FIGURE 14. Carboxylic acid terminated nanoparticles and amine-functionalized random copolymer used in the ternary assembly processes.

enables both binary MMPC−polymer and ternary MMPC−polymer−MMPC assembly processes, with aggregation controlled through both component stoichiometry and by order of addition in the stepwise assembly process.

We used carboxylic acid terminated nanoparticles Au-COOH **14** and SiO_2-COOH **16** (synthesized from SiO_2-NH_2 using maleic anhydride) as the building blocks, and an amine-functionalized random copolymer poly-NH_2 **17** served as the "mortar" (Figure 14). A great diversity of structural motifs and aggregate sizes is observed using this ternary assembly strategy.[25] Most importantly, the order of addition of the components allows the creation of either composites in which the nanoparticles are well integrated (Figure 15a) or segregated colloid clusters (Figure 15b).

While our previous studies demonstrated interesting structures, our goal is to make catalysts! To demonstrate the ability of our assembly strategy to fabricate high-efficiency catalysts, we replaced the Au-COOH **14** nanoparticles with Pd-COOH **18**, which were synthesized with the same ligands in a similar fashion.[26] The palladium colloid was added to a preformed **SiO_2-COOH/poly-NH_2** aggregate in order to reach a high concentration of the catalytic metal on the surface of the final composite. The porous aggregates were calcinated at 500 °C, resulting in complete removal of all organic matter (according to thermal gravimetry analysis (TGA)). TEM micrographs of the calcinated systems reveal that the high porosity of the systems remained intact (Figure 16).

The catalytic activity of calcinated Pd-COOH/SiO_2-COOH/poly-NH_2 was quantified through hydrogenation of 9-decen-1-ol. The observed turnover frequencies (TOF, calculated as $mol_{product}\ mol_{Pd}^{1-}\ h^{-1}$), measured at the mass transport limit,[26] were as high as 10 100 h^{-1} (for the 1:1:1

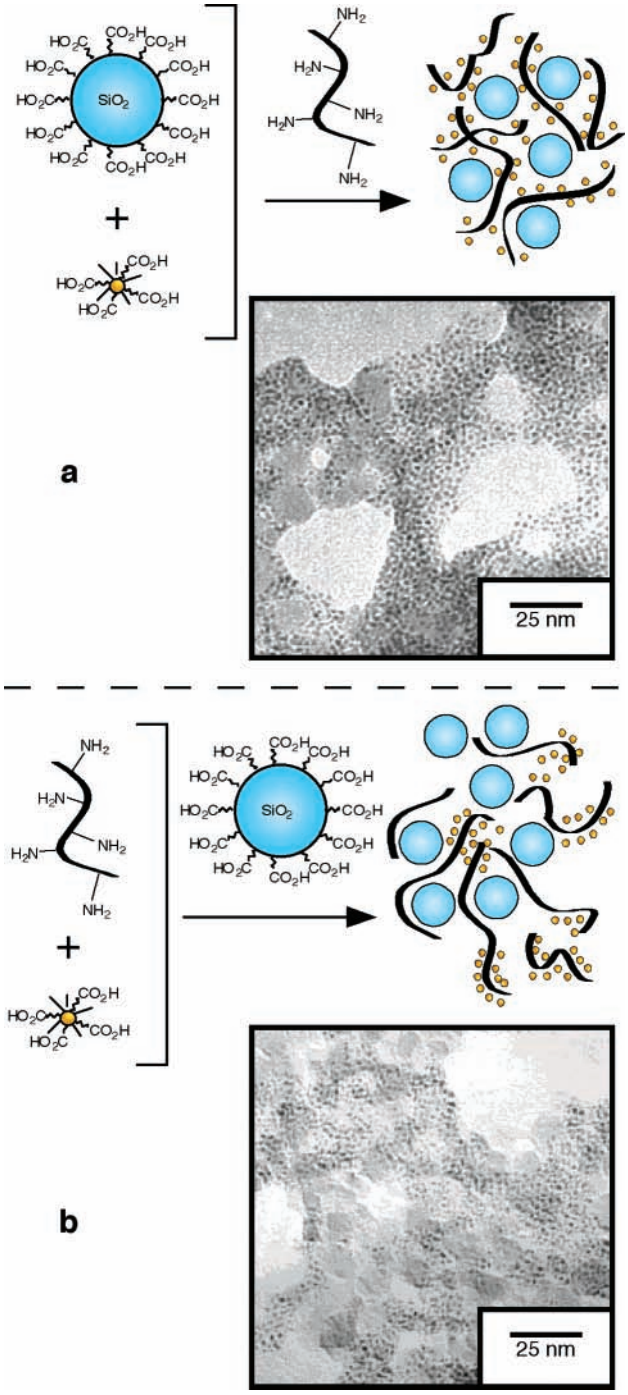

FIGURE 15. The dependence between order of assembly and resulting aggregate structure in ternary systems. Au-COOH/SiO_2-COOH/poly-NH_2 ratios in TEM images are 3:1:4 (a) and 1:1:2 (b), respectively.

w/w/w composition of Pd/Si/polymer, respectively),[27] a substantial increase compared to the 7200 h^{-1} found under the same conditions for the widely employed commercial 1% Pd/C catalyst, and competitive with other state of the art supported nanostructured catalysts.[23a] Additionally, the nanocomposite catalyst was highly efficient for Heck coupling reactions between electronically activated bromoarenes and styrene or methyl acrylate, reactions for which Pd/C and Pd/SiO_2 are quite inefficient.

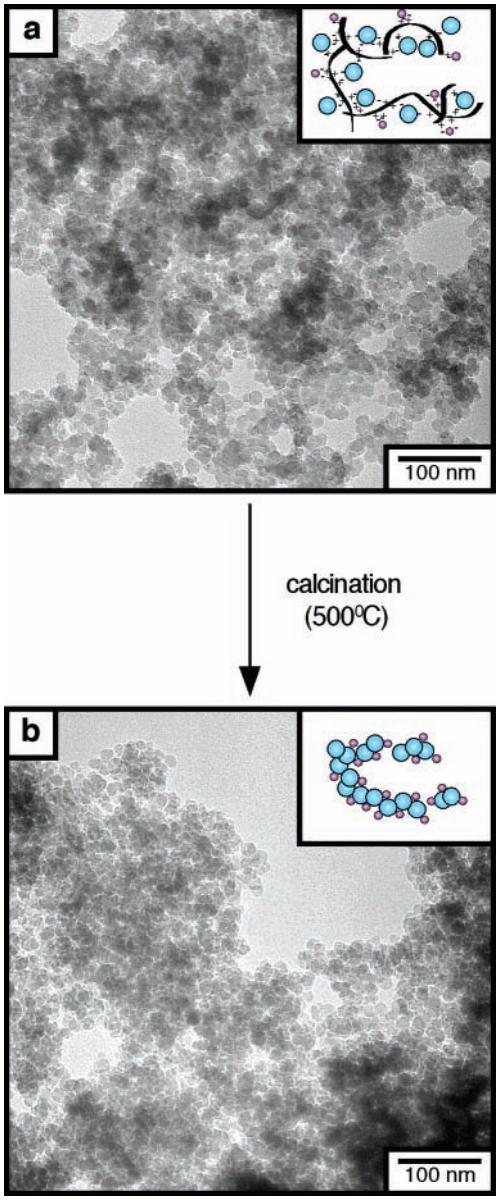

FIGURE 16. Porosity retention (a) before and (b) after calcination of a 1:1:1 Pd-COOH/SiO_2-COOH/poly-NH_2 composite. Insets: schematical illustrations of corresponding aggregates.

Most importantly, the catalyst requires no activation and can be recycled with only a small decrease in activity.[26]

The bottom-up approach shown here lays a framework for the development of new, highly efficient catalysts, which can be finely tuned to the desired application. We are currently exploring the extension of this approach for the creation of additional catalytic and biocatalytic systems.

B. Organized Nanoparticle Assemblies. Highly structured, three-dimensional nanocomposites possess unique magnetic, electronic, and optical properties, providing new systems for the creation of devices and sensors.[28] In our research we have been investigating methods for extending the diversity of molecular assembly methods to nanoparticle systems. The same polymer-mediated "bricks and mortar" approach described above was employed for this purpose; however, this time we used complementary recognition units (instead of ionic interactions) as the driving force for assembly.[29] The balance between entropy and enthalpy in these systems allows assembly under near-equilibrium conditions, which facilitates error (defect) correction. This attribute, coupled with the ability of the flexible polymer to compensate for shape irregularities, allows the propagation of structure to larger scales through the self-assembly process.

In our initial studies, we employed diaminotriazine-thymine three-point hydrogen-bonding interaction to obtain complementarity between thymine-functionalized colloids Thy-Au **20** and diaminotrazine-functionalized polystyrene poly-Triaz[30] **19** (Figure 17a). Black solid was formed immediately after poly-Triaz was added to concentrated solutions of Thy-Au in nonpolar solvents. In contrast, no precipitation was observed when the control colloid MeThy-Au **21** is used, demonstrating the crucial role of specific hydrogen-bonding interactions in the formation of poly-Triaz/Thy-Au aggregates. TEM images of the THF-soluble fraction of the poly-Triaz/Thy-Au precipitate revealed the formation of large spherical clusters (Figure 17c). These highly regular aggregates are comprised of 3000−7000 individual gold particles per microsphere, and range 97 ± 17 nm in diameter. The gold nanoparticles within the microsphere are separated by 6.4 ± 0.3 nm (center-to-center) as determined by small-angle x-ray scattering (SAXS). This value agrees with a 4.4 nm edge-to-edge separation distance determined by molecular modeling (Figure 17b).

The temperature at which the aggregation process was performed had a profound effect on the assembly process. At 10 °C, networks of larger, highly size-dispersed spherical aggregates were formed (Figure 17d). These are apparently intermediate structures; performing the aggregation at −20 °C yielded even larger, yet again individual clusters (Figure 17e). These giant clusters are 5−10 times larger than the aggregates formed at 23 °C, ranging 0.5−1.0 μm in diameter and comprising of 0.6−5.0 million individual Thy-Au nanoparticles. These microscale aggregates are among the most complex synthetic self-assembled structures known, demonstrating the thermal control of aggregate size using the bricks and mortar methodology.

The boundary of the assembly process is dictated presumably by surface tension of the resulting aggregate. While allowing some control over aggregates dimensions, this method is indirect and highly sensitive to local effects. To directly control the cluster size, we employed as the mortar three symmetric diblock copolymers **22**−**24** with varying total lengths (Figure 18).[31] Here, the aggregate growth is restricted by the diblock copolymer inherent feature of micro-phase separation; the final size is determined by the functionalized block length (Figure 19).

The resulting aggregates show a clear dependence between the polymer length and the aggregate size (Figure 20). Moreover, a significant improvement in cluster size-dispersity is observed (<10%, compared to ∼ 17% with clusters formed with monoblock poly-Triaz). The average core sizes calculated from the TEM images are 50−70% of the effective hydrodynamic radii (R_h) determined by

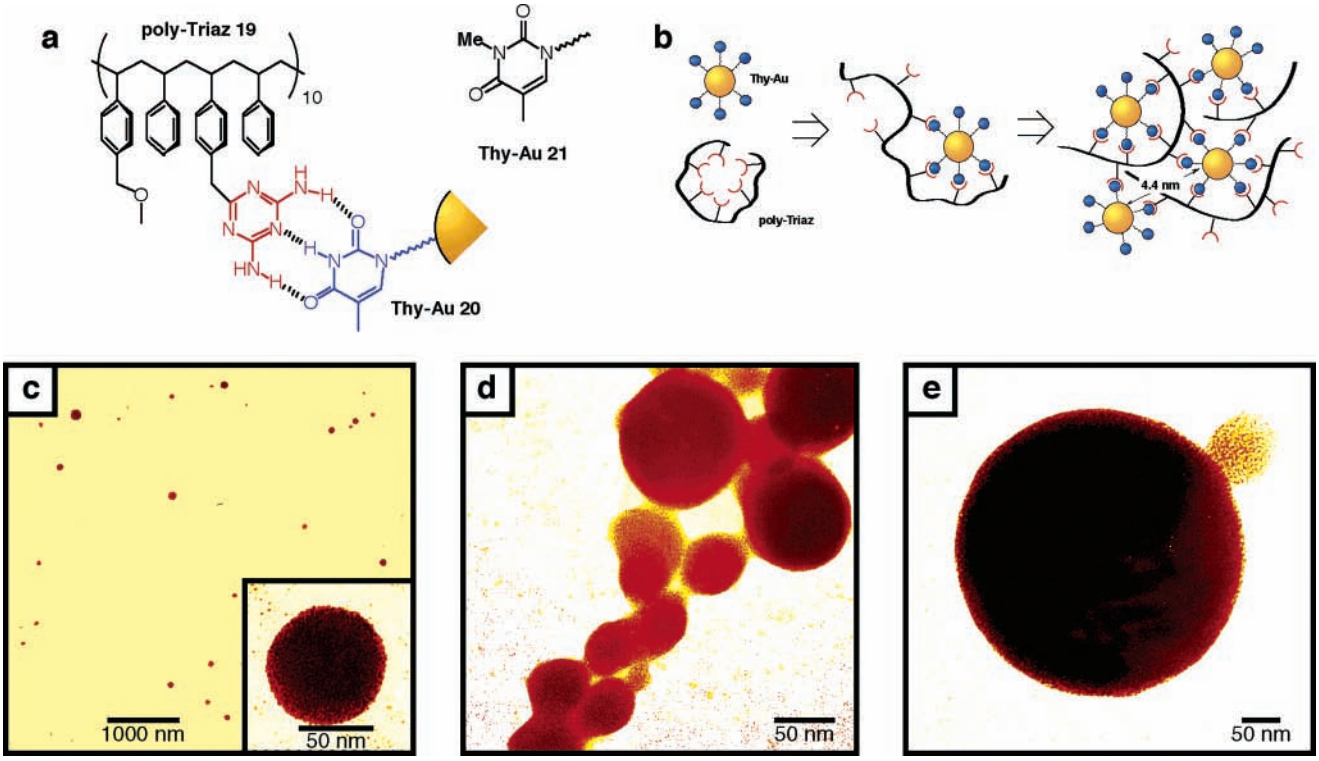

FIGURE 17. (a) Recognition between diaminotriazine-functionalized polymer and thymine-capped nanoparticle. (b) Suggested mechanism of Thy-Au/poly-Triaz aggregation.[29] TEM micrographs of Thy-Au/poly-Triaz aggregates formed at (c) 23 °C (Inset: representative microsphere), (d) 10 °C, (e) −20 °C.

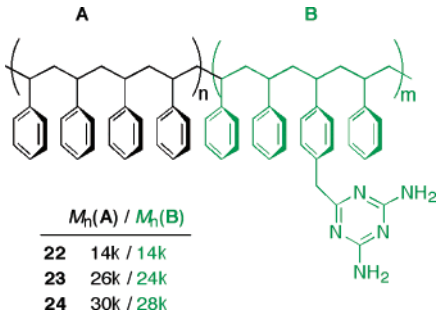

	M_n(A) / M_n(B)
22	14k / 14k
23	26k / 24k
24	30k / 28k

FIGURE 18. Diblock copolymers used to control aggregate dimensions.

dynamic light scattering (DLS) for the combined core and corona (Figure 20d). This suggests that the polymer chains within the core are somewhat extended relative to the polystyrene corona.

Interparticle spacing is an important assembly parameter that serves a crucial role in determining nanoparticle behavior within assemblies.[2] To control spacing between Au-COOH **14** nanoparticles, we employed poly(amidoamine) (PAMAM) dendrimers **25**−**29** of different generations (G_0- G_6) as the mortar units (Figure 21a).[32] SAXS experiments revealed a clear correlation between particle−particle spacing ($d = 2\pi/q$) and the dendrimer generation

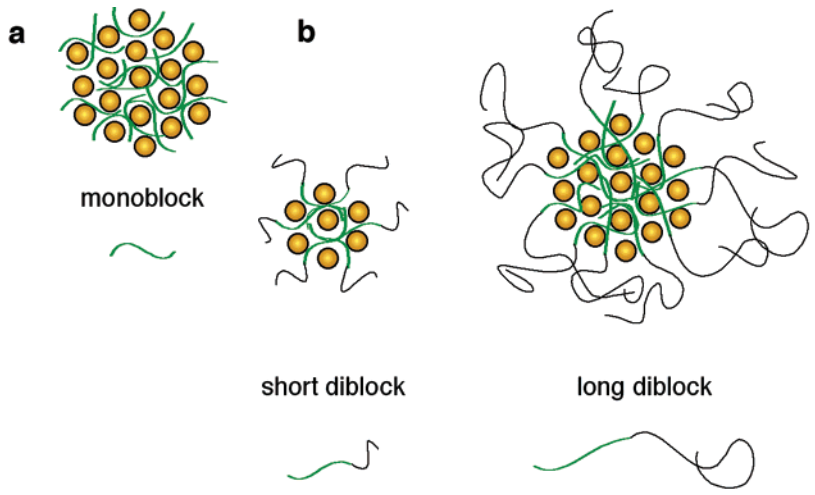

FIGURE 19. Illustrated comparison between aggregate size and type of polymer used: (a) With mono-block polymers, cluster size is dictated presumably by surface tension. (b) With diblock copolymers, the functionalized-block length controls aggregate size.

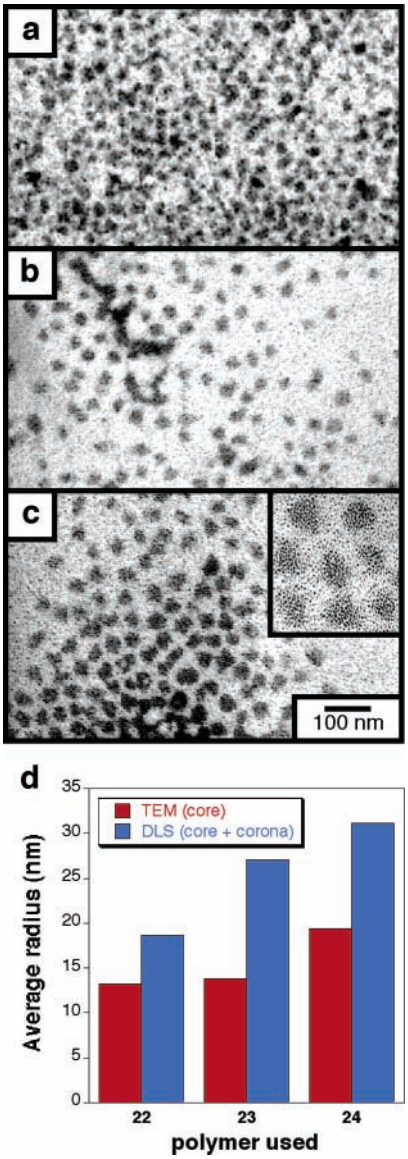

FIGURE 20. TEM micrographs of spherical micellar structures formed by assembly of Thy-Au with polymers **22** (a), **23** (b), and **24** (c; inset, 2× magnification showing individual MMPCs inside the aggregates). (d) Comparison between average core sizes calculated from TEM images and hydrodynamic radii determined by DLS.

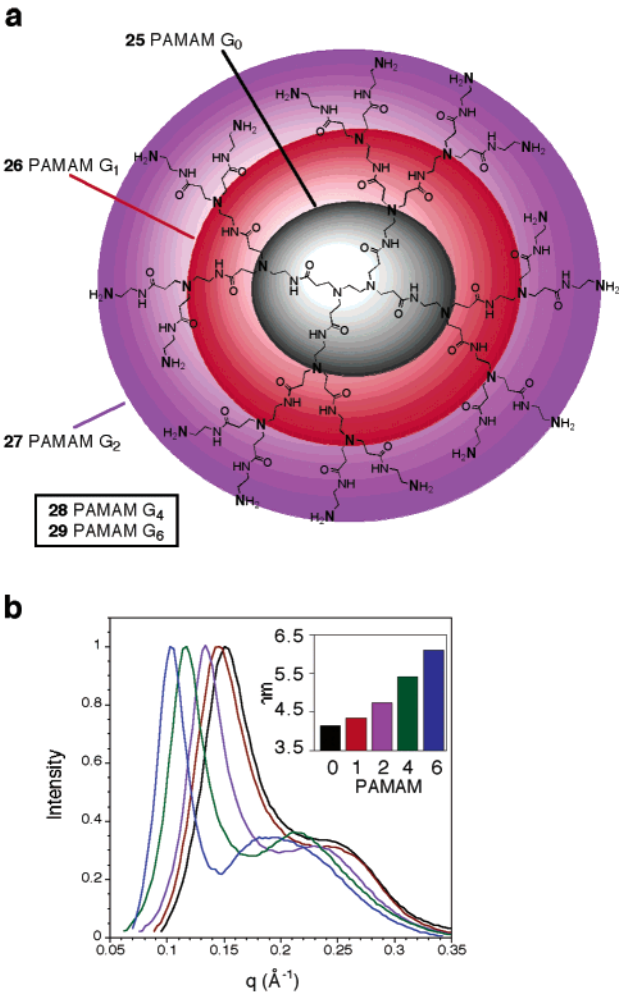

FIGURE 21. (a) PAMAM dendrimers **25**−**29**. (b) SAXS plot of Au-COOH **14** assembled with G_0-G_6 PAMAM dendrimers. Inset: dependence of spacing on dendrimer generation.

(Figure 21b). A broad second-order peak is observed in all cases, which implies medium-range ordering. The ratio of the maxima q values between the secondary and main peaks moves gradually from ∼1.7 for G_0 dendrimer **25** to ∼2 for G_6 dendrimer **29**. These values suggest internal packing structure that is intermediate between solid and liquid models (ratio of $\sqrt{2}$ and 2, respectively), with packing order tendency toward liquid packing model with increasing dendrimer generation.

We are currently working on expanding the repertoire of aggregate compositions. One direction is the replacement of the polymeric moiety with other types of components. The tendency of certain chemical functionalities to crystallize may serve as a different type of gluing mortar in this sense. Polyoligosilsequioxane (POSS) is such a unit: it is a nanoscopic building block (∼1.5 nm in diameter), which can be easily modified, and has a high tendency to crystallize.[33] In a recent study, we combined the hydrogen-bonding recognition strategy for assembly of nanoparticle with the crystallizing tendency of POSS building blocks to create a novel type of large-scale assemblies.[34] When Thy-Au **20** is mixed with POSS-DAP **30** (a POSS nanoparticle functionalized with DAP recognition element), well-defined spherical aggregates of 250 nm−1.5 μm in diameter are formed (Figure 22a). The center-to-center distances between the gold particles observed with SAXS is 3.65 ± 0.08 nm, corresponding to an edge-to-edge distance of ca. 2.1 nm. This distance implies a side-to-side packing arrangement of the POSS units (Figure 22b); a face-to-face arrangement would have lead to a substantially larger spacing (∼4.5 nm).

The formation of discrete regular aggregates of different compositions and controlled size and shape provides the initial step on the way to controlled nanoparticle assembly. We are currently exploring methods to expand our control of aggregate morphologies,[35] as well as the modification of other useful nanoparticles and building blocks (e.g., magnetic γ-Fe_2O_3 nanoparticles[36]) in order to use them in our assembly scheme for advanced applications.

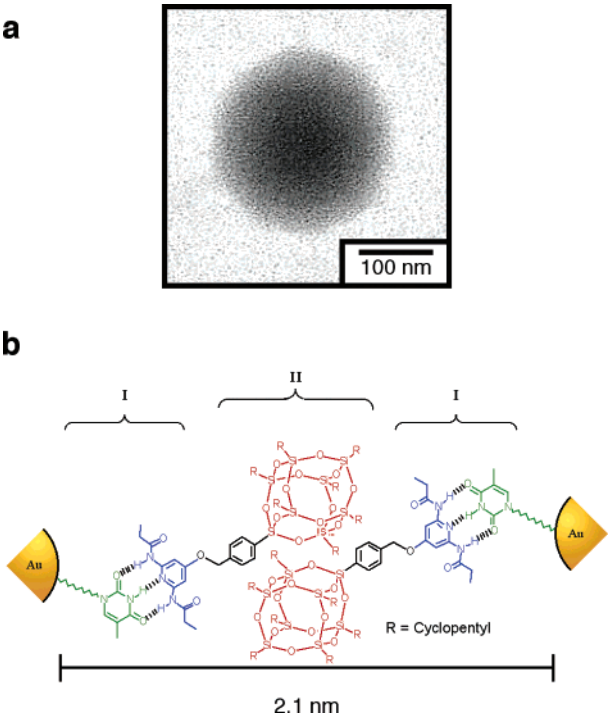

FIGURE 22. (a) Spherical aggregate of POSS-DAP with Thy-Au. (b) Representation of the hydrogen bonding (I) and crystalline (II) domains in the aggregates of POSS-DAP/Thy-Au.

Summary and Outlook

Control of nanoparticle properties provides opportunities for the de novo creation of unique systems. The nanoparticle scaffold, with its radial tunability and inherent balance between kinetics and thermodynamics, provides a unique tool for the creation of catalysts, sensors, and devices. The ability to control the assembly of these systems into varied morphologies extends this versatility to the creation of nanocomposite systems. The examples given in this Account hint at an almost endless horizon of potential applications: solution-based sensors for small molecules, molecular shuttles for specific drug-delivery, chemotherapeutic drugs, electrically stimulated devices, highly efficient catalysts, nano-metric magnetic assemblies for high-density read-write media, stimuli-responsive surfaces, scaffolds for layer-by-layer construction, and more. Nevertheless, further investigation is still required in order to achieve these important goals. Once we know how to translate the rules of molecular-level function tailoring into precise shape, size, and property of a large-scale complex system, we will have a truly powerful tool for the fabrication of pragmatic systems.

The research described herein was sponsored by the NIH, NSF, Research Corporation, The Sloan Foundation, and the Dreyfus Foundation.

References

(1) Jager, E. W. H.; Smela, E.; Inganas, O. Microfabricating Conjugated Polymer Actuators. *Science* **2000**, *290*, 1540−1545. Craighead, H. G. Nanoelectromechanical Systems. *Science* **2000**, *290*, 1532−1535. Wallraff, G. M.; Hinsberg, W. D. Lithographic Imaging Techniques for the Formation of Nanoscopic Features. *Chem. Rev.* **1999**, *99*, 1801−1821.

(2) Feldheim, D.; Grabar, K. C.; Natan, M. J.; Mallouk, T. E. Electron Transfer in Self-Assembled Inorganic Polyelectrolyte/Metal Nanoparticle Heterostructure. *J. Am. Chem. Soc.* **1996**, *118*, 7640−7641, and references therein.

(3) Templeton, A. C.; Wuelfing, M. P.; Murray, R. W. Monolayer Protected Cluster Molecules. *Acc. Chem. Res.* **2000**, *33*, 27−36.

(4) Brust, M.; Walker, M.; Bethell, D.; Schiffrin, D. J.; Whyman, R. Synthesis of Thiol-Derivatized Gold Nanoparticles in a 2-Phase Liquid−Liquid System. *J. Chem. Soc., Chem. Commun.* **1994**, 801−802.

(5) Hostetler, M. J.; Wingate, J. E.; Zhong, C.-J.; Harris, J. E.; Vachet, R. W.; Clark, M. R.; Londono, J. D.; Green, S. J.; Stokes, J. J.; Wignall, G. D.; Glish, G. L.; Porter, M. D.; Evans, N. D.; Murray, R. W. Alkanethiolate Gold Cluster Molecules with Core Diameters from 1.5 to 5.2 nm: Core and Monolayer Properties as a Function of Core Size. *Langmuir* **1998**, *14*, 17−30.

(6) Templeton, A. C.; Hostetler, M. J.; Warmoth, E. K.; Chen, S. W.; Hartshorn, C. M.; Krishnamurthy, V. M.; Forbes, M. D. E.; Murray, R. W. Gateway Reactions to Diverse, Polyfunctional Monolayer-Protected Gold Clusters. *J. Am. Chem. Soc.* **1998**, *120*, 4845−4849.

(7) Boal, A.; Rotello, V. *Intra*- and *Inter*-Monolayer Hydrogen bonding in Amide Functionalized Alkanethiol SAMs on Gold Nanoparticles. *Langmuir* **2000**, *16*, 9527−9532.

(8) Paulini, R.; Frankamp, B. L.; Rotello, V. M. Effects of Branched Ligands on the Structure and Stability of Monolayers on Gold Nanoparticles. *Langmuir* **2002**, *18*, 2368−2373.

(9) Templeton, A. C.; Hostetler, M. J.; Kraft, C. T.; Murray, R. W. Reactivity of Monolayer-Protected Gold Cluster Molecules: Steric Effects. *J. Am. Chem. Soc.* **1998**, *120*, 1906−1911. Weisbecker, C. S.; Merritt, M. V.; Whitesides, G. M. Molecular Self-Assembly of Aliphatic Thiols on Gold Colloids. *Langmuir* **1996**, *12*, 3763−3772.

(10) Tam-Chang, S.-W.; Biebuyck, H. A.; Whitesides, G. M.; Jeon, N.; Nuzzo, R. G. Self-Assembled Monolayers on Gold Generated from Alkanethiols with the Structure $RNHCOCH_2SH$. *Langmuir* **1995**, *11*, 4371−4382. Clegg, R. S.; Hutchison, J. E. Control of Monolayer Assembly Structure by Hydrogen Bonding Rather Than by Adsorbate−Substrate Templating. *J. Am. Chem. Soc.* **1999**, *121*, 5319−5327.

(11) Hostetler, M. J.; Templeton, A. C.; Murray, R. W. Dynamics of Place-Exchange Reactions on Monolayer-Protected Gold Cluster Molecules. *Langmuir* **1999**, *15*, 3782−3789.

(12) Briggs, C.; Norsten, T. B.; Rotello, V. M. Inhibition and Acceleration of Deuterium Exchange in Amide-Functionalized Monolayer-Protected Gold Clusters. *Chem. Commun.* **2002**, 1890−1891.

(13) Kirby, A. J.; Percy, J. M. The Hydrogen-Bond as a Key Factor in Efficient Intramolecular Proton-Transfer Catalysis. *J. Chem. Soc., Chem. Commun.* **1987**, 1774−1775.

(14) Boal, A. K.; Rotello, V. M. Redox-Modulated Recognition of Flavin by Functionalized Gold Nanoparticles. *J. Am. Chem. Soc.* **1999**, *121*, 4914−4915. For a previous example of recognition at a gold nanoparticle surface using a diaminopyridine-imide dyad, see: Aherne D.; Rao S. N.; Fitzmaurice D. Programming a gold nanocrystal to recognize and selectively bind a molecular substrate in solution *J. Phys. Chem. B* **1999**, *103*, 1821−1825.

(15) Niemz, A.; Rotello, V. M. From Enzyme to Molecular Device. Exploring the Interdependence of Redox and Molecular Recognition. *Acc. Chem. Res.* **1999**, *32*, 44−52.

(16) Binding constants of reduced species are obtained through the relation $K_a(\text{red})/K_a(\text{ox}) = \exp[(nF/RT)(E_{1/2(\text{bound})} - E_{1/2\ (\text{unbound})}]$.

(17) Boal, A. K.; Rotello, V. M. Fabrication and Self-Optimization of Multivalent Receptors on Nanoparticle Scaffolds. *J. Am. Chem. Soc.* **2000**, *122*, 734−735.

(18) Boal, A. K.; Rotello, V. M. Radial Control of Recognition and Redox Processes with Multivalent Nanoparticle Hosts. *J. Am. Chem. Soc.* **2002**, *124*, 5019−5024.

(19) Badia, A.; Cuccia, L.; Demers, L.; Morin, F.; Lennox, R. B. Structure and Dynamics in Alkanethiolate Monolayers Self-Assembled on Gold Nanoparticles: A DSC, FT-IR and ^{2}H-NMR Study. *J. Am. Chem. Soc.* **1997**, *119*, 2682−2692.

(20) McIntosh, C. M.; Esposito, E. A.; Boal, A. K.; Simard, J. M.; Martin, C. T.; Rotello, V. M. Inhibition of DNA Transcription Using Cationic Mixed Monolayer Protected Gold Clusters. *J. Am. Chem. Soc.* **2001**, *123*, 7626−7629.

(21) Fischer N. O., McIntosh C. M., Simard J. M., Rotello V. M. Inhibition of Chymotrypsin Through Surface Binding Using Nanoparticle-Based Receptors. *P. Natl. Acad. Sci. U.S.A.* **2002**, *99*, 5018−5023.

(22) Loweth, C. J.; Caldwell, W. B.; Peng, X. G.; Alivisatos, A. P.; Schultz, P. G. DNA-Based Assembly of Gold Nanocrystals. *Angew. Chem., Int. Ed. Engl.* **1999**, *38*, 1808−1812. Mirkin, C. A.; Letsinger, R. L.; Mucic, R. C.; Storhoff, J. J. A DNA-Based Method for Rationally Assembling Nanoparticles into Macroscopic Materials.

Nature **1996**, *382*, 607−609. Shenton, W.; Davis, S. A.; Mann, S. Directed Self-Assembly of Nanoparticles into Macroscopic Materials using Antibody−Antigen Recognition. *Adv. Mater.* **1999**, *11*, 449−453.
(23) (a) Thomas, J. M.; Johnson, B. F. G.; Raja, R.; Sankar, G.; Midgley. P. A. High-Performance Nanocatalysts for Single-Step Hydrogenations *Acc. Chem. Res.* **2003**, *36*, 20−30. (b) Aiken, J. D.; Finke, R. G. A Review of Modern Transition-Metal Nanoclusters: Their Synthesis, Characterization, and Applications in Catalysis. *J. Mol. Catal. A: Chem.* **1999**, *145*, 1−44.
(24) Galow, T. H.; Boal, A. K.; Rotello, V. M. A 'Building Block' Approach to Mixed-Colloid Systems through Electrostatic Self-Organization. *Adv. Mater.* **2000**, *12*, 576−579.
(25) Boal, A. K.; Galow, T. H.; Ilhan, F.; Rotello, V. M. Binary and Ternary Polymer-Mediated 'Bricks and Mortar' Self-Assembly of Gold and Silica Nanoparticles. *Adv. Funct. Mater.* **2001**, *11*, 461−465.
(26) Galow, T. H.; Drechsler, U.; Hanson, J. A.; Rotello, V. M. Highly Reactive Heterogeneous Heck and Hydrogenation Catalysts Constructed through 'Bottom-Up' Nanoparticle Self-Assembly. *Chem. Commun.* **2002**, 1076−1077.
(27) Increasing polymer fraction in the process of making the catalysts was found to lower the TOF (7600 h^{-1} for the 1:1:5 system), consistent with a denser structures observed with such systems.
(28) Shipway, A. N.; Katz, E.; Willner, I. Nanoparticle Arrays on Surfaces for Electronic, Optical and Sensor Applications. *ChemPhysChem* **2000**, *1*, 18−52. Murray, C. B.; Kagan, C. R.; Bawendi, M. G. Synthesis and Characterization of Monodisperse Nanocrystals and Close-Packed Nanocrystal Assemblies. *Annu. Rev. Mater. Sci.* **2000**, *30*, 545−610.
(29) Boal, A. K.; Ilhan, F.; DeRouchey, J. E.; Thurn-Albrecht, T.; Russell, T. P.; Rotello, V. M. Self-Assembly of Nanoparticles into Structured Spherical and Network Aggregates. *Nature* **2000**, *404*, 746−748.
(30) Deans, R.; Ilhan, F.; Rotello, V. M. Recognition-Mediated Unfolding of a Self-Assembled Polymeric Globule. *Macromolecules* **1999**, *32*, 4956−4960.
(31) Frankamp, B. L.; Uzun, O.; Ilhan, F.; Boal, A. K.; Rotello, V. M. Recognition-Mediated Assembly of Nanoparticles into Micellar Structures with Diblock Copolymers. *J. Am. Chem. Soc.* **2002**, *124*, 892−893.
(32) Frankamp, B. L.; Boal, A. K.; Rotello, V. M. Controlled Interparticle Spacing through Self-Assembly of Au Nanoparticles and Poly(amidoamine) Dendrimers. *J. Am. Chem. Soc.* **2002**, *124*, 15146−15147.
(33) Zheng, L.; Waddon, A. J.; Farris, R. J.; Coughlin, E. B. X-ray Characterizations of Polyethylene Polyhedral Oligomeric Silsesquioxane Copolymers. *Macromolecules* **2002**, *35*, 2375−2379.
(34) Carroll, J. B.; Frankamp, B. L.; Rotello, V. M. Self-Assembly of Gold Nanoparticles through Tandem Hydrogen bonding and POSS−POSS Recognition Processes. *Chem. Commun.* **2002**, 1892−1893.
(35) Boal, A. K.; Gray, M.; Ilhan, F.; Clavier, G. M.; Kapitzky, L.; Rotello, V. M. Bricks and Mortar Self-Assembly of Nanoparticles. *Tetrahedron* **2002**, *58*, 765−770.
(36) Boal, A. K.; Das, K.; Gray, M.; Rotello, V. M. Monolayer Exchange Chemistry of γ-Fe_2O_3 Nanoparticles. *Chem. Mater.* **2002**, *14*, 2628−2636.

AR020083J